

# Metal Independent Correlations for Site-specific Binding Energies of Relevant Catalytic Intermediates

Shyama Charan Mandal<sup>‡,†</sup> and Frank Abild-Pedersen<sup>†,\*</sup>

<sup>‡</sup>SUNCAT Center for Interface Science and Catalysis, Department of Chemical Engineering,  
Stanford University, 443 Via Ortega, Stanford, CA 94305, USA

<sup>†</sup>SUNCAT Center for Interface Science and Catalysis, SLAC National Accelerator Laboratory,  
2575 Sand Hill Road, Menlo Park, CA 94025, USA

\*E-mail: [abild@slac.stanford.edu](mailto:abild@slac.stanford.edu)

## Abstract

Establishing energy correlations among different metals can accelerate the discovery of efficient and cost-effective catalysts for complex reactions. Using a recently introduced coordination-based model, we can predict site specific metal binding energies ( $\Delta E_M$ ) that can be used as a descriptor for chemical reactions. In this study, we have examined a range of metals including Ag, Au, Co, Cu, Ir, Ni, Os, Pd, Pt, Rh, and Ru and found linear correlations between predicted  $\Delta E_M$  and adsorption energies of CH and O ( $\Delta E_{CH}$  and  $\Delta E_O$ ) at various coordination environment for all the considered metals. Interestingly, all the metals correlate with one another under specific surface site coordination, indicating that different metals are interrelated in a particular coordination environment. Furthermore, we have tested and verified for PtPd and PtIr-based alloys that they follow a similar behavior. Moreover, we have expanded the metal space by taking some early transition metals along with few s-block metals and shown a cyclic behavior of the adsorbate binding energy ( $\Delta E_A$ ) versus  $\Delta E_M$ . Therefore,  $\Delta E_{CH}$  and  $\Delta E_O$  can be efficiently interpolated between metals, alloys and intermetallics based on information related to one metal only. This simplifies the process of screening new metal catalyst formulations and their reaction energies.

**Keywords:** Density function theory; coordination-based  $\alpha$ -scheme model; binding energies; metal independent correlation; hydrocarbon-based adsorbates; sigmoid function

## 1. Introduction

Heterogeneous catalysis plays a critical role in advancing sustainability within chemical reactions. Platinum group elements (PGE) have been extensively utilized for various thermal and electrochemical reactions such as the hydrogen evolution reaction, the oxygen reduction reaction and hydrocarbon combustion reactions.<sup>1-7</sup> The limited availability of catalysts based on PGE and their high costs pose a barrier to the widespread adoption and use at large scale.<sup>8</sup> In addition, there is still significant room for improvement in catalytic activity and product selectivity. To overcome these challenges and enhance sustainability in chemical reactions, more cost-effective and efficient catalyst alternatives are needed. In this context, numerous detailed experimental and theoretical studies have shed light on this topic.<sup>9-16</sup> A combination of experimental insight and theoretical investigations is needed to provide valuable understanding in heterogeneous catalysis. Utilizing density functional theory (DFT) to calculate reaction energies and activation energies, we can rationalize the activity, selectivity, and stability of a catalyst surface. However, the identification of efficient catalysts remains a time-consuming and tedious process since catalysts are dynamic under operation requiring feedback between experimental and theoretical efforts.<sup>17</sup> To speed up the process, recent advancements in machine learning and artificial intelligence have been utilized in catalysis.<sup>18</sup> But these approaches often lack the ability to provide a comprehensive understanding of the fundamental properties of the catalyst and how to link these to observations for fluctuating systems. Hence, it is of utmost importance to develop a comprehensive model which accurately and efficiently combine input based on information about the local structure of

the catalyst.<sup>19,20</sup> Such models would not only expedite the catalyst screening process but also provide a solid foundation for understanding catalysis at the fundamental level. In recent years, remarkable advancements have been made in establishing links between adsorption energies.<sup>21–23</sup> Such approaches significantly reduce efforts and screening time for catalysts. Recently, a coordination-based model, known as the  $\alpha$ -scheme model, was constructed with the goal to predict the binding energy of an active surface site ( $\Delta E_M$ ) in a diverse coordination environment.<sup>24,25</sup> Armed with this new descriptor, we have successfully demonstrated correlations with adsorption energies of various hydrocarbon-based adsorbates along with CO and OH and efficiently linked a vast number of hydrocarbon-based adsorbates in simple classification scheme.<sup>22,26</sup> The recent classification of adsorbates was performed specifically on Pt and in this paper, we aim to expand the framework to include other transition metals. Crucially, all these findings are strongly correlated with the site stability, leading us to introduce a novel descriptor,  $\Delta E_M$ , for catalysis.

In this study, we have investigated the correlation of various metals on a specific surface site coordination starting from an  $\alpha$ -scheme model predicted  $\Delta E_M$  (Figure 1). A wide range of metals including Ag, Au, Co, Cu, Ir, Ni, Os, Pd, Pt, Rh, and Ru were examined, and a statistically significant number of calculations were used to extrapolate the  $\alpha$ -parameters for each metal to accurately predict  $\Delta E_M$ . We have chosen CH and O as relevant intermediates due to their key role in a wide range of hydrocarbon- and steam-based reactions.<sup>21,22,27</sup> We demonstrate strong correlations among all the metals at a specific coordination environment enabling us to efficiently predict and understand the behavior of different metals in similar coordination environments, contributing to the advancement of catalyst design and optimization for sustainable chemical reactions. We have also tested our model for alloys and found that it follows a similar behavior as observed for metals. We expanded the screened metal space to include early transition metals as

well as s-block metals and as expected we find a periodic behavior of the  $\Delta E_A$  versus  $\Delta E_M$  as we gradually empty the atomic orbitals.

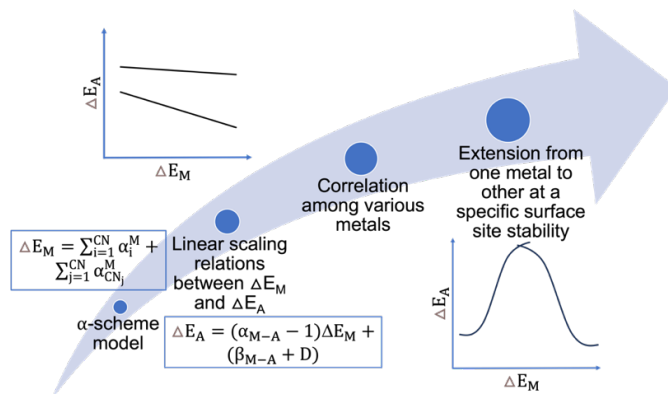


**Figure 1:** This schematic figure illustrates a step-by-step process for understanding metal binding energies ( $\Delta E_M$ ) and their metal correlation for a specific surface site coordination. The coordination-based  $\alpha$ -scheme model can predict  $\Delta E_M$  and shows how the binding energies of adsorbate ( $\Delta E_A$ ) exhibit a linear scaling relationship with  $\Delta E_M$ . Various metals are correlated with each other for a specific surface site coordination.

## 2. Computational details

The Vienna Ab initio Simulation Package (VASP) was utilized in conjunction with the Atomic Simulation Environment (ASE) to carry out all the first principles density functional theory (DFT) calculations.<sup>28–31</sup> To incorporate exchange-correlation effects, we have considered the BEEF-vdW functional,<sup>32,33</sup> a well-established method that has been extensively validated for calculating adsorbate binding energies on metal surfaces.<sup>22,34</sup> The plane wave basis sets were employed during optimization were set with a cutoff energy of 500 eV. To ensure accurate results, all structures were optimized until the total energies converged to a minimum of  $10^{-5}$  eV, and the forces reached a threshold of less than 0.05 eV/Å. The metal lattice constants utilized in this study were obtained from earlier reports<sup>22,24,34</sup> or calculated using equation of state computational approaches. The optimized lattice constants for each metal at face-centered cubic (fcc) lattice are as follows: Ag

4.22 Å, Au 4.20 Å, Co 3.46 Å, Cu 3.68 Å, Ir 3.88 Å, Ni 3.55 Å, Os 3.86 Å, Pd 3.98 Å, Pt 3.98 Å, Rh 3.85 Å, and Ru 3.81 Å. For the binding energy calculations, we employed 7 layers of  $3 \times 3$  M(100) and  $3 \times 3$  M(111), whereas for (211) we have considered 7 layers of  $1 \times 3$  slabs. In all the structures the bottom four layers were kept fixed, while the remaining layers were allowed to relax during the system optimization process. The considered adsorbate CH and O have been adsorbed on the ontop site of metals. To mitigate periodic image interactions, a significant vacuum region of more than 15 Å was introduced between the slabs in the z-direction. The Monkhorst Pack method was employed to generate appropriate k-point grids within the Brillouin zone.<sup>35</sup> For the reciprocal space of the surfaces, a  $4 \times 4 \times 1$  k-point grid was utilized to solve the DFT-based Kohn-Sham equations. Furthermore, to eliminate any artificial periodic interactions between the slabs, dipole corrections were applied.<sup>36</sup> The gas phase molecules have been optimized within a  $21 \text{ Å} \times 22 \text{ Å} \times 23 \text{ Å}$  cell. A  $1 \times 1 \times 1$  k-point density has been used during the optimization of the gas phase molecules. To calculate the metal or adsorbate binding energies, we used the following equation (1a and 1b):

$$\Delta E_M = E_{\text{slab}+M} - (E_{\text{slab}} + E_M) \quad (1a)$$

$$\Delta E_A = E_{\text{slab}+A} - (E_{\text{slab}} + E_A) \quad (1b)$$

In the above equation (1a and 1b),  $\Delta E_M$  and  $\Delta E_A$  represents the binding energy of metal and adsorbate,  $E_{\text{slab}+M}$  and  $E_{\text{slab}+A}$  represents the total energy of the slab with metal (M), and total energy of the slab with adsorbate (A),  $E_{\text{slab}}$  is the total energy of the slab, and  $E_M$  is the total energy of metal (M) whereas  $E_A$  is the total energy of adsorbate (A). All the structures and binding energies can be found in cathub (<https://www.catalysis-hub.org/publications/MandalMetal2024>).<sup>37</sup>

### 3. Results and discussion

In the following section we discuss (i) the choice of metals and validation of  $\alpha$ -scheme model, (ii) the correlation of metal binding energies with adsorbate binding energies ( $\Delta E_M$  vs.  $\Delta E_A$ ), (iii) the correlation among different metals and maximum binding energies for specific adsorbates, and finally we validate our model for alloys and expand it beyond the transition metals to illustrate the periodic behavior of the  $\Delta E_A$  versus  $\Delta E_M$ . This helps establish simple and useful correlations for various metals within specific coordination environments.

### 3.1. Choice of metals and validation of $\alpha$ -scheme model

To establish the necessary correlations, we have explored site binding energies,  $\Delta E_M$ , within a given coordination environment. We have focused on a selection of relevant transition metals, namely Ag, Au, Co, Cu, Ir, Ni, Os, Pd, Pt, Rh, and Ru. These metals have been selected due to their significance in catalytic reactions, rendering them highly relevant to our investigation. Recent studies have extensively utilized most of these metals in a variety of essential reactions. For instance, Ag, Au, Ni, Cu, and Ru are successfully used for di-hydrogen bond activation,<sup>38–40</sup> while Pt, Ru, Ni, Co, and Rh have shown promise for C–H bond activation in hydrocarbon chemistry.<sup>41–43</sup> Additionally, Pt is important because of its efficiency in the hydrogen evolution reaction,<sup>7,44</sup> hydrocarbon combustion,<sup>4,45</sup> and oxygen reduction reaction,<sup>46,47</sup> while Ir excels in the oxygen evolution reaction,<sup>48,49</sup> and Cu is recognized for its potential in CO<sub>2</sub> reduction reaction.<sup>50,51</sup> However, to further enhance the catalytic activity and reduce costs, researchers have extensively explored the catalytic activity of cheaper metals and compositions thereof. Throughout our study, we have placed specific emphasis on analyzing the behavior of these metals within the face-centered cubic (fcc) crystal structure. After carefully considering the selection of metals, we proceeded to evaluate our coordination-based  $\alpha$ -scheme model using the BEEF-vdW functional.

According to the  $\alpha$ -scheme model the metal binding energies can be predicted from the identity of the metal atom and its coordination number changes. Hence, the energy of the considered metal atom can be represented as  $E_n^Z$  with a metal Z in coordination environment n. To obtain  $E_n^Z$  we consider the energy of every coordination environment from a few number of DFT calculations where energy of every coordination environment can be represented via  $\alpha_i^Z$ . The whole set of coordination environment can be obtain from twelve  $\alpha_i^Z$  values  $\alpha_{1-3}^Z, \alpha_4^Z, \alpha_5^Z, \dots, \alpha_{11}^Z, \alpha_{12,100}^Z, \alpha_{12,111}^Z, \alpha_{12,bulk}^Z$ . In this context, we did not consider any separate  $\alpha_1^Z, \alpha_2^Z$  and  $\alpha_3^Z$  values and hence the value  $\alpha_{1-3}^Z$  is the combination of these three values where  $\alpha_{1-3}^Z = \alpha_1^Z + \alpha_2^Z + \alpha_3^Z$ . Moreover, we have considered three different  $\alpha_{12}^Z$  values for 100, 111 and bulk as they are different even if they have same coordination number. Once all of these twelve  $\alpha_i^Z$  values are known we can predict the metal binding energies at any environment. It is important to mention that we consider only the first nearest neighbor of the considered site as the consideration of second sphere of the coordination number has very little effect to the metal binding energies. For example, if a metal atom is bonded on 111 surface with a coordination number 3 then the metal atom get coordination number 3 whereas the surrounding 3 atoms coordination number is 10 hence the binding energy of the metal ( $\Delta E_M$ ) at coordination number 3 on 111 surface can be represented as addition of  $\alpha_{1-3}^Z$  and three  $\alpha_{10}^Z$  ( $\alpha_{1-3}^Z + 3\alpha_{10}^Z$ ). To obtain the  $\alpha$ -values, we performed a statistically significant number of DFT calculations (18 binding energy calculations) for each individual metal.<sup>22,24</sup> In this study, the  $\alpha$ -values were calculated relative to the bulk energy of the metal atoms, as accurately calculating gas phase energies of these atoms using DFT can be challenging and we would like to compare the results from one metal to another. Therefore, we chose to use the face-centered cubic (fcc) bulk energy of metal atoms as the reference point during  $\Delta E_M$  calculations. Whenever we consider the energy of bulk metal atoms as a reference, as opposed

to the gas phase energy of the metal, we essentially subtract the cohesive energy of the metal from the gas phase energy. Therefore, in all cases, the binding energy of the metal can be represented by the following equation:

$$\Delta E_M = E_M^i - E_M^{coh} \quad (2)$$

In the above equation (2)  $\Delta E_M$  is the binding energy of the considered metal with respect to the bulk energy of that respective metal,  $E_M^i$  is the binding energy of the metal atom  $i$  with respect to gasphase and  $E_M^{coh}$  is the cohesive energy of the metal. The binding energy of a metal atom in a given coordination environment can be derived using only twelve  $\alpha$ -parameter values:  $\alpha_{1-3}^Z$ ,  $\alpha_4^Z$ ,  $\alpha_5^Z$ ,  $\alpha_6^Z$ ,  $\alpha_7^Z$ ,  $\alpha_8^Z$ ,  $\alpha_9^Z$ ,  $\alpha_{10}^Z$ ,  $\alpha_{11}^Z$ ,  $\alpha_{12,bulk}^Z$ ,  $\alpha_{12,100}^Z$  and  $\alpha_{12,111}^Z$ . Based on the  $\alpha$ -scheme model we can obtain  $\Delta E_M$  by considering the changes in the coordination environment. Let's consider, we are interested to obtain the metal binding energy of a metal atom on 100 surface which is showing a coordination number of 4 whereas surrounding four atoms coordination number is 9. Hence, the metal binding energy based on the bond strength will be  $\alpha_{1-3}^Z + \alpha_4^Z + 4\alpha_9^Z$ . The similar approaches have been shown earlier in case of coordination number 3 on 111 surface. Hence, the general expression for obtaining the metal binding energy will be  $\sum_{i=1}^{CN} \alpha_i^M + \sum_{j=1}^{CN} \alpha_{CNj}^M$ , where the corresponding  $\alpha$ -values are pre-established based on the 18 binding energies. This approach has been established by considering gas phase energy of the metal atom. To obtain the metal binding energy with respect to the bulk energy of the system we subtract cohesive energy of the metal. Based on the  $\alpha$ -scheme model cohesive energy of the system can be derived by summing all the  $\alpha$ -values, i.e.,  $\sum_{i=1}^{12} \alpha_i^M$  for fcc bulk structures. Hence, by combining these two aspects, we can derive the following equation representing  $\Delta E_M$  concerning the bulk metal as a reference:

$$\Delta E_M = \sum_{i=1}^{CN} \alpha_i^M + \sum_{j=1}^{CN} \alpha_{CNj}^M - \sum_{i=1}^{12} \alpha_i^M \quad (3)$$

Figure 2 illustrates the integral plot of all the  $\alpha$ -values for increasing coordination. A complete list of these  $\alpha$ -values is provided in the supporting information Table S1. When extracting the  $\alpha$ -values using 18 binding energy calculations for each metal we obtain the following MAE values: Ag: 0.023 eV, Au: 0.041 eV, Co: 0.054 eV, Cu: 0.032 eV, Ir: 0.111 eV, Ni: 0.042 eV, Os: 0.148 eV, Pd: 0.039 eV, Pt: 0.062 eV, Rh: 0.053 eV, Ru: 0.092 eV. Among all the metals, the highest MAE was observed for Os, 0.148 eV, and the lowest MAE was found for Ag, 0.023 eV. Once determined, these  $\alpha$ -parameters can be applied effectively to various structures within the complete set of metals, eliminating the need for redundant calculations in other applications. With this coordination-based model, we are now able to accurately predict the  $\Delta E_M$  using the  $\alpha$  values which directly reflect the coordination environment of the respective metals. The same has been shown in earlier reports.<sup>22,24,26</sup>

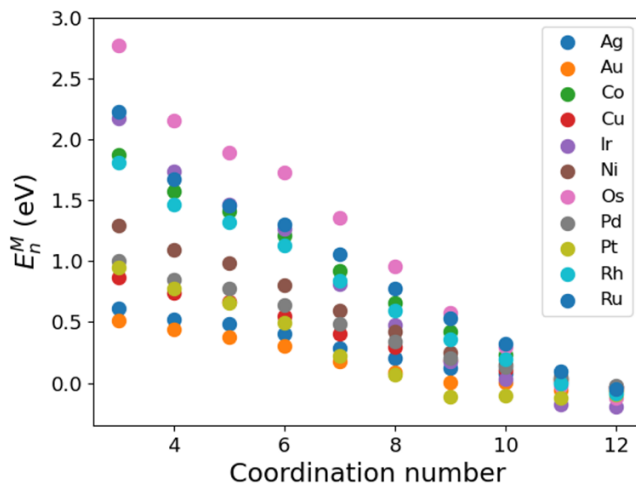


**Figure 2:** Fcc metal atoms energies as a function of their coordination number. The energy values were obtained through calculations using the bond associated  $\alpha_i^Z$  parameters.  $\alpha_{12}^M$  is the average value of  $\alpha_{12,bulk}^Z$ ,  $\alpha_{12,100}^Z$  and  $\alpha_{12,111}^Z$ . This simple framework significantly enhances the practicality and applicability of our model, allowing us to make reliable predictions for a wide range of scenarios without the need for repeated computations. The  $\alpha$ -scheme model was employed to predict  $\Delta E_M$ , and a comparison was made with DFT-calculated  $\Delta E_M$  for all the metals under consideration. The resulting data is shown in

Figure S1 in the supplementary information. The figures demonstrate good agreement and hence justification for applying the  $\alpha$ -scheme model in predicting  $\Delta E_M$  across all the metals examined. This level of accuracy in predicting the binding energy through the established model further substantiates the reliability and robustness of our approach.

### 3.2. Correlation of metal binding energies with adsorbate binding energies ( $\Delta E_M$ vs. $\Delta E_A$ )

In agreement with earlier studies, we find that binding energies of hydrocarbon-based adsorbates ( $\Delta E_A$ ) follow a linear correlation with the  $\alpha$ -predicted metal binding energies ( $\Delta E_M$ ).<sup>22,26</sup> The linear scaling relationship between the binding energy of adsorbates and the metal binding energies anticipated by the  $\alpha$ -scheme model can be expressed through the following equation (4):

$$\Delta E_A = (\alpha_{M-A} - 1)\Delta E_M + (\beta_{M-A} + D) \quad (4)$$

In equation (4), the coefficient  $\alpha_{M-A} - 1$  represents the binding strength of the adsorbates on the catalytic surface and the two intercept parameters  $\beta_{M-A} + D$  are associated with the gas phase complexes. To verify the applicability of the correlation to the considered adsorbate (CH and O) binding energies and the descriptor  $\Delta E_M$ , a selection of data points was employed, encompassing a range of  $\alpha$ -scheme predicted metal binding energies. These points span from low metal coordination (weak metal binding energy) to high metal coordination (strong metal binding energy). The  $\Delta E_M$  in some cases are positive and for some cases it's negative. For example, the metal binding energy for coordination number 4 is positive whereas the same is showing negative in the case of coordination number 9. This is due to consideration of the considered metal atom's coordination number as well as coordination number of the surrounding metal atoms. The metal binding energy equation of the considered coordination number 4 structure (Figure 3a) is  $\alpha_{1-3}^Z + \alpha_4^Z + 4\alpha_{10}^Z$  whereas the metal binding energy equation of the considered coordination number 9

(Figure 3e) is  $\alpha_{1-3}^Z + \alpha_4^Z + \alpha_5^Z + \alpha_6^Z + \alpha_7^Z + \alpha_8^Z + 7\alpha_9^Z + 3\alpha_{12,111}^Z$ . Based on the  $\alpha$ -parameters (Table S1), we get a positive metal binding energy for coordination number 4 and negative metal binding energy for coordination number 9. In case of atop adsorption of CH and O we have considered five data points on each metal ranging from coordination number 4 to coordination number 9 (Figure 3a-e). All the above-mentioned structures were considered for obtaining the linear scaling relations for  $\Delta E_A$  vs.  $\Delta E_M$  when A=CH or O. It is important to note that the  $R^2$  of the linear scaling relationships approaches unity by introducing more data points. However, we have already shown that these linear scaling relationships hold for various  $\Delta E_A$  with respect to the  $\alpha$ -scheme predicted  $\Delta E_M$ .<sup>22,26</sup> Nonetheless, the linear scaling relationships derived from this subset of points exhibit a high degree of consistency in agreement with earlier observations.<sup>22</sup> Therefore, it is anticipated that the considered data points would suffice to establish accurate linear scaling relationships between the  $\Delta E_A$  and  $\Delta E_M$ .

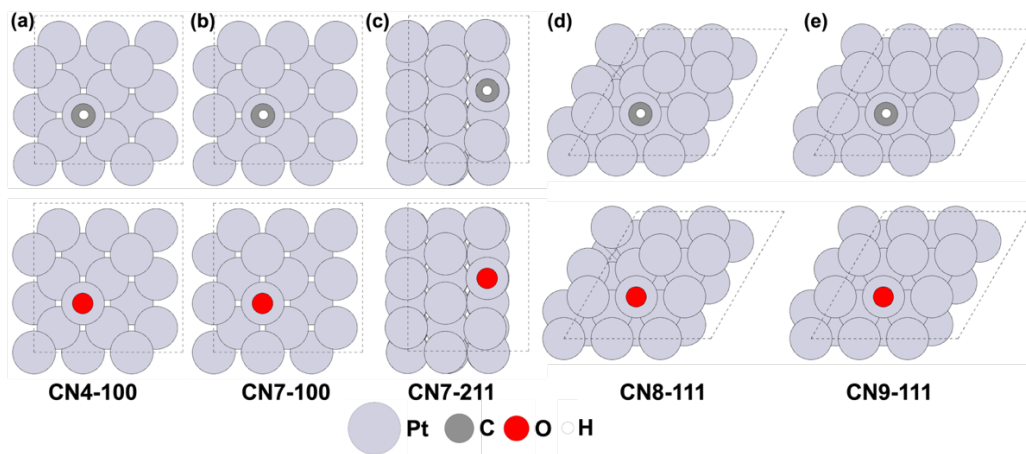


**Figure 3:** (a-e) Model structures applied to establish the linear correlations between the DFT calculated  $\Delta E_A$  (A=CH and O) and the  $\alpha$ -predicted  $\Delta E_M$ . The  $\Delta E_M$  with respect to the bulk metal energy values were obtained using bond-associated  $\alpha_i^Z$  parameters.

In Figure 4a and 4b, we summarize the linear scaling relations between the DFT energies  $\Delta E_{CH}$  and  $\Delta E_O$  vs.  $\Delta E_M$ , respectively. The details of the linear relations such as slopes, intercepts and

mean absolute errors can be found in Table S2 of the supporting information. The observed linear scaling relationships provide strong evidence that  $\Delta E_M$  serves as an accurate and efficient predictor for  $\Delta E_A$ . It is important to note that the slopes and intercepts of these linear scaling relationships exhibit specific variations. The values of slopes and intercepts within the linear scaling relationships are contingent upon both the metal's identity and the nature of the adsorbates. In most of the cases, the slopes are negative which means that increasing site stability  $\Delta E_M$  leads to a decreasing adsorbate binding  $\Delta E_A$  and vice versa. These findings align with the results reported in earlier publications.<sup>22</sup> Surprisingly, when examining the case of CH adsorption on the ontop site, we find that the slope for  $\Delta E_{CH}$  versus  $\Delta E_M$  is positive for the coinage 3d and 4d metals Ag and Cu, almost zero for 3d and 4d metals Pd, Ni, Ru, Rh, and Pd, and negative for all the 5d metals. This observation indicates that the presence of the CH adsorbate leads to a stabilization of the coinage 3d and 4d metals, a near structure independent behavior on the remaining 3d and 4d metals, and strong structure dependence on the 5d metals. In case of O adsorption, only Ag shows a surface stabilizing effect, Cu a near structure independent adsorption, whereas the remaining metals display strong structure dependence.

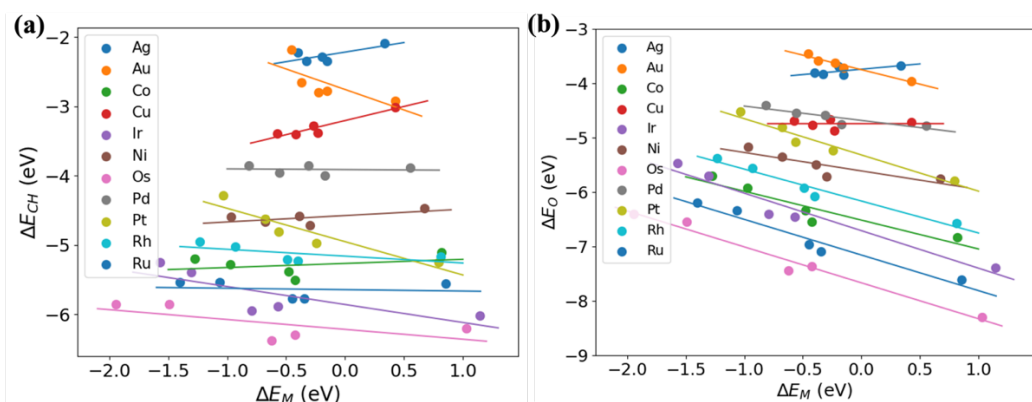


**Figure 4:** The DFT-calculated adsorbate energies  $\Delta E_A$  have been plotted against the surface site stability  $\Delta E_M$  predicted using the  $\alpha$ -scheme. Site stabilities are referenced to the energy of bulk metal atoms. (a) shows ontop adsorption energies  $\Delta E_{CH}$  versus  $\Delta E_M$  adsorption, and (b) shows ontop adsorption energies  $\Delta E_O$  versus  $\Delta E_M$  adsorption.

### 3.3. Correlation among various metals at a given coordination environment

In this section, we study the intricate relationships that exist between adsorption on specific coordination numbers and the various transition metals. Our investigation results in a metal-independent correlation among the binding energies of CH and O ( $\Delta E_{CH}$  and  $\Delta E_O$ ) versus the predicted site stabilities  $\Delta E_M$  as illustrated in Figure 5. We observe that the adsorption energy ceases to increase further for a coordination specific site stability  $\Delta E_M$ . Clearly, this is anticipated since energy scaling relations are based on the existence of an optimum electronic density, thus resulting in a maximum binding  $\Delta E_A$  for a given adsorbate. In this paper, we are focusing primarily on late transition metals but as we shall see later, the chosen descriptor  $\Delta E_M$  and its periodicity when filling a single orbital, has consequences for the correlations. The cohesive energy of transition metals according to Friedel follow a second order behavior as a function of d-filling, hence  $\Delta E_M$  reaches its minimum value when  $f_d = 0.5$ .<sup>52</sup> Where  $f_d$  is the fractional filling of the d-shell. Based on our observations we shall assume that for the late transition metals the site dependent correlation among various metals follow a sigmoid function with a specific maximum and minimum points. We have considered sigmoid function based on the maximum and minimum adsorbate binding energies with respect to the metal binding energies. Besides, the sigmoid behavior can be used in two different directions based on the positive and negative metal binding energies. The maximum and minimum adsorption energies strongly depend on the surface site and the specific adsorbate. For a given adsorbate the range of adsorption energies increase with decreasing coordination of the adsorbed site and the maximum and minimum values can be approximated based on the  $\Delta E_A$ . When fitting the sigmoid function, we have allowed for minimum and maximum values with an absolute variation of 0.10 eV and during the curve fitting the

maximum and minimum binding energies are kept fixed within that range for all the considered adsorbates. The sigmoid function is given by the following equation (5):

$$\Delta E_A = \Delta E_A^{min/max} + (\Delta E_A^{max/min} - \Delta E_A^{min/max}) / (1 + \exp(-b * (\Delta E_M - c))) \quad (5)$$

$\Delta E_A^{min}$  and  $\Delta E_A^{max}$  is the maximum and minimum adsorption energies at a specific surface site stability, respectively,  $b$  is the rate parameter, and  $c$  is descriptor value at the inflection point.

Because of the definition of  $\Delta E_M$  and its strong dependence on coordination number, the  $c$ -value in the sigmoid function changes sign leading to the transition from an s-curve to an inverted s-curve at lower coordination.

Interestingly, there should exist an effective coordination number leading to a Heaviside step function with  $\left. \frac{\partial \Delta E_A}{\partial \Delta E_M} \right|_{\Delta E_M=0} = \infty$ .

Given we know the  $\Delta E_M$  for a given coordination number we can now approximate the adsorption energy  $\Delta E_A$  from the fitted sigmoid curves.

We have listed the parameters for the optimized sigmoid functions for adsorbates CH and O in Table S3 of the supporting information.

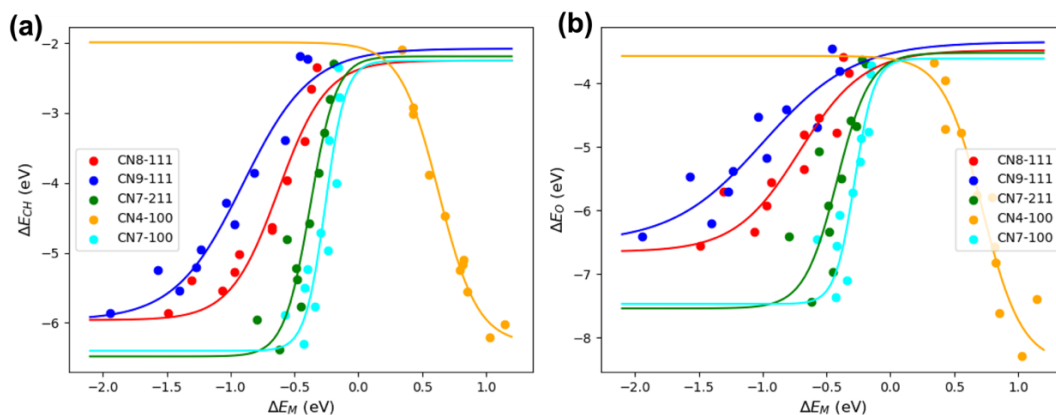


**Figure 5:** Calculated adsorption energies of (a)  $\Delta E_{CH}$  and (b)  $\Delta E_O$  plotted against the predicted  $\Delta E_M$ . The fitting curves show coordination specific metal independent correlations for all the considered late transition metals.

In addition to exploring the pure metal-based systems, we have also investigated the usability of the correlations for alloys. We have specifically examined PtPd- and PtIr-based alloys in the case of CN4-100. The model structures are illustrated in Figure S2 of the supporting information. We

determined the metal binding energies and CH adsorption energies for these systems using DFT calculations. We used the bulk cohesive energy of Pt as reference for the metal binding energies. The results are summarized in Figure 6a, and we note that the binding energies of CH on PtPd and PtIr-based alloys do not follow the same trend found for the pure metal-based systems. Since applying the bulk energy of clean Pt as a reference for the stability of Pt atoms in the alloys is insufficient and no direct DFT calculations can provide such values. To validate our model, we have first extracted the reference metal binding energy in that specific configuration from the best fitted sigmoid function of  $\Delta E_M$  versus  $\Delta E_{CH}$ . In the next step, we have considered the same structures (Figure S2) and the obtained  $\Delta E_M$  for the prediction of alloy-based O adsorption energies (Figure 6b). In the case of  $\Delta E_M$  versus  $\Delta E_O$  the prediction of O adsorption energies matches well with the pure metal-based sigmoid function. Combining the corrected reference energies of the metal with calculated adsorption energies of O on the alloy systems we find the adsorption energy  $\Delta E_O$  to strongly agree with the correlation established for the pure metals (Figure 6b). To summarize, if we know the correct reference of  $\Delta E_M$ , the metal independent correlations can be expanded to include alloys and intermetallics as well.

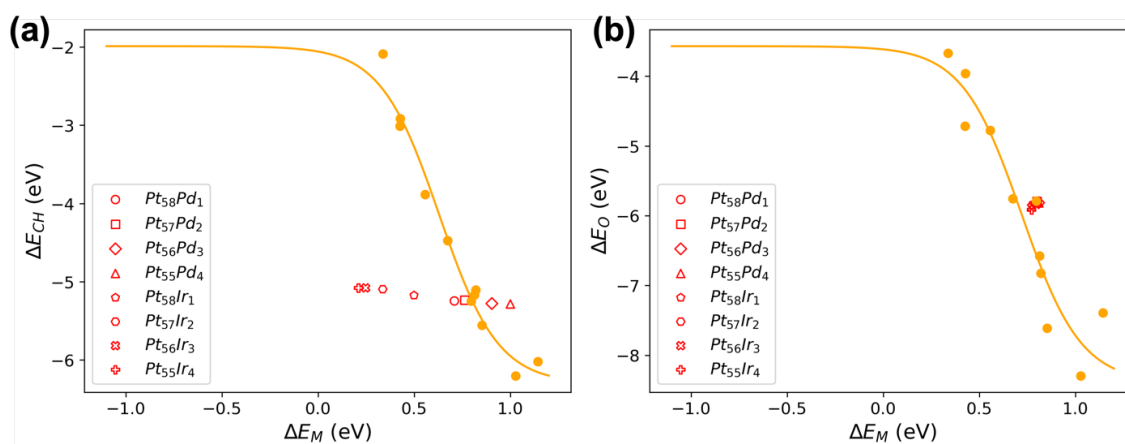


**Figure 6:** Calculated adsorption energies of (a)  $\Delta E_{CH}$  plotted against the calculated  $\Delta E_M$  and (b) calculated adsorption energies of  $\Delta E_O$  versus predicted  $\Delta E_M$ . Where  $\Delta E_M$  specifically for the alloy systems have been corrected using results

from (a). Solid and open symbols are for pure metals and alloy-based systems, respectively. The solid curves represent the metal independent correlations optimized for the pure metal systems on CN4-100.

In this final section, we expand our investigation to include early 4d transition metals and 5s metals. Explicitly, we considered Rb, Sr, Y, Zr, Nb, Mo, Tc, Ru, Rh, Pd, Ag, and Cd metals in an fcc crystal structure to obtain a comprehensive understanding of the periodic behavior of adsorption strength versus  $\Delta E_M$ . We use the ontop adsorption of CH on close-packed 111 surfaces (CN9-111) as our model structures and have calculated  $\Delta E_M$  relative to the bulk metal energies. Because of the periodic trend in the cohesive energies when you fill up subshell, as shown in Figure 7a, the descriptor  $\Delta E_M$  will reflect a similar behavior, and the correlation functions introduced cannot be injective for the domain consisting of all metals in the periodic table as seen from Figure 7b. In this context, the cohesive energy of the metals follows Friedel second order behavior. The separation of the metals in Figure 7b is also based on the d-filling ( $f_d$ ) of the metals. The first sigmoid is for Rb to Tc which is considering d-filling up to 0.5 whereas the second sigmoid curve is from  $f_d = 0.6$  to 1 for Ru Rh, Pd, Ag, and Cd. We have divided our correlation of  $\Delta E_{CH}$  versus  $\Delta E_M$  into two functions based on the cohesive energy curve in Figure 7a. The range of metals from Rb to Tc follows one sigmoid curve where  $\Delta E_{CH}$  increases from its minimum to its maximum binding strength and for the range of metals from Ru to Cd where the cohesive energy is decreasing,  $\Delta E_{CH}$  reverts back to its minimum energy along a different sigmoid curve as shown in Figure 7b. The cyclic behavior of  $\Delta E_{CH}$  versus  $\Delta E_M$  for ontop adsorption close-packed (111) surface is a consequence of changes in cohesive energy and the bond strength of the adsorbate, where  $\Delta E_M$  reflect the cohesive energy behavior, and the bond strength is related to the d-band characteristics of the metals. Along with the ontop adsorption of the CH, we have tested our model for CH hollow adsorption (Figure S3). The predicted  $\Delta E_M$  are the average of the considered hollow site. The results show that the predicted  $\Delta E_M$  show a strong correlation with the  $\Delta E_{CH}$  at various

coordination environment for a specific metal. Moreover, there is correlation among various metals at a specific surface site coordination. Hence, the proposed model can be expanded for various other adsorption sites. Because of the generic behavior also at different coordination numbers, we anticipate similar cyclic nature for other coordination environments, other metal subshells, and for other adsorbates. These insights will provide a valuable tool to better understand the relationship between surface structure and activity and serve as guidance for researchers and engineers in the fields of surface science and catalysis.

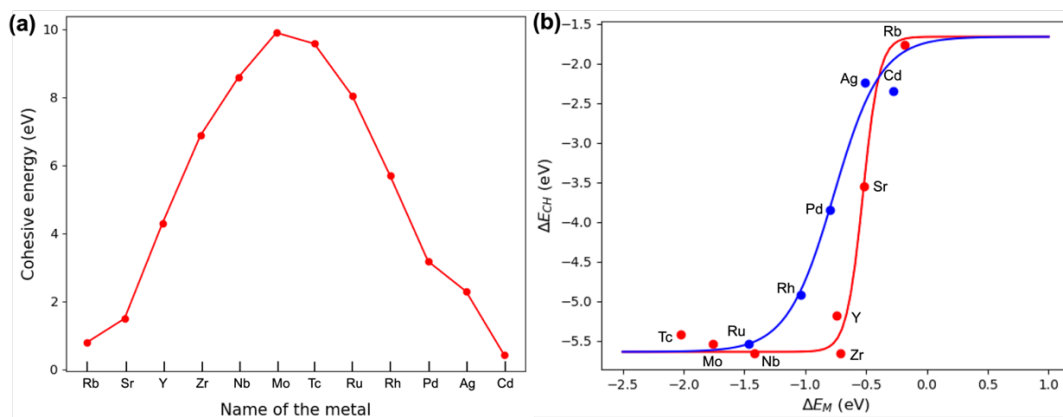


**Figure 7:** (a) Calculated cohesive energies plotted for 5s and 4d transition metals. (b) Calculated binding energies for ontop adsorption of CH,  $\Delta E_{CH}$ , on close-packed (111) surfaces plotted against the site-specific metal binding energy,  $\Delta E_M$ , referenced to the bulk cohesive energy of the metal. The solid red curve is best sigmoid fit to metals Rb, Sr, Y, Zr, Nb, Mo and Tc whereas the blue solid curve is best sigmoid fit to metals Ru, Rh, Pd, Ag, and Cd. All  $\Delta E_M$  for these systems has been calculated using DFT.

#### 4. Conclusions

We have investigated the metal independent correlation of  $\Delta E_M$  versus  $\Delta E_A$  ( $A = CH$  and O) at specific surface site coordination for a range of metals (Ag, Au, Co, Cu, Ir, Ni, Os, Pd, Pt, Rh, and Ru). The coordination-based  $\alpha$ -scheme model has been applied to predict  $\Delta E_M$  and we have investigated the linear scaling relations between  $\Delta E_M$  and  $\Delta E_A$  at various coordination

environments. All the considered metals show strong linear scaling relations between  $\Delta E_A$  and  $\Delta E_M$  throughout the considered metal coordination environments. For a specific surface site coordination  $\Delta E_A$  show a correlation with  $\Delta E_M$  for different metals within a site-specific maximum and minimum energy range. The correlations are best fitted by either sigmoid or reverse sigmoid functions depending on site coordination, and it suggest that a specific coordination number exists where the correlation is a step function at  $\Delta E_M=0$ . In the case of alloy-based system, we considered PtPd and PtIr-based alloys and investigated the system independent correlation. In this case, obtaining correct cohesive energies is highly challenging and we explicitly considered one specific system (CH adsorption data) to obtain the correct cohesive energy references. Applying these reference energies to investigate O adsorption data for the same systems we found that the model indeed can be used for alloy and intermetallic systems as well. In addition, we have expanded our model by including data points on early transition metals as well as some s-block elements. Interestingly, the correlation shows a cyclic behavior with respect to the  $\Delta E_M$ . This is due to the introduction of the cohesive energy term within the  $\Delta E_M$  which follows a second order behavior as a function of d-filling. Overall, our model enables us to find out the correlation among various metals and alloys at specific surface site coordination. We believe that the model can be expanded further, and because of its versatility can lead to a much broader application.

### **Associated Content**

**Supporting Information:** The  $\alpha_i^Z$  values of considered metals including corrections for subsurface, comparison of  $\alpha$ -scheme model predicted and DFT calculated  $\Delta E_M$ , linear fitting parameters along with mean absolute errors of  $\Delta E_A$  versus  $\Delta E_M$  for all the considered metals where

adsorbates are CH and O, sigmoid fitting equations at a specific surface site stability for various metals using predicted  $\Delta E_M$  versus DFT calculated  $\Delta E_{CH}$  and  $\Delta E_O$ , considered PtPd and PtIr alloy-based structures at CN4-100.

## **Acknowledgement**

We acknowledge support from the U.S. Department of Energy, Office of Science, Office of Basic Energy Sciences, Chemical Sciences, Geosciences, and Biosciences Division, Catalysis Science Program to the SUNCAT Center for Interface Science and Catalysis. This research used resources of the National Energy Research Scientific Computing Center; a DOE Office of Science User Facility supported by the Office of Science of the U.S. Department of Energy under Contract No. DE-AC02-05CH11231 using NERSC award BES-ERCAP0024127. We acknowledge computational support from the SLAC Scientific Data Facility (SDF).

## **Data availability**

A detailed list of DFT energies and structures is provided via the catalysis-hub.org repository<sup>37</sup> at <https://www.catalysis-hub.org/publications/MandalMetal2024>. The uploaded metal binding energies are with respect to the gasphase metal energies. To get the metal binding energies with respect to bulk we just need to add 2.3315 eV, 2.8379 eV, 6.2614 eV, 3.2219 eV, 8.2122 eV, 4.8444 eV, 10.2433 eV, 3.2039 eV, 5.3803 eV, 5.7123 eV, 8.0630 eV, 0.7979 eV, 1.5048 eV, 4.3132 eV, 6.8903 eV, 8.6009 eV, 9.9139 eV, 9.5918 eV and 0.4430 eV for Ag, Au, Co, Cu, Ir, Ni, Os, Pd, Pt, Rh, Ru, Rb, Sr, Y, Zr, Nb, Mo, Tc and Cd metals, respectively.

## **References**

- (1) Savignan, L.; Faucher, S.; Chéry, P.; Lespes, G. Platinum Group Elements Contamination in Soils: Review of the Current State. *Chemosphere* **2021**, *271*, 129517.
- (2) McCrory, C. C. L.; Jung, S.; Ferrer, I. M.; Chatman, S. M.; Peters, J. C.; Jaramillo, T. F. Benchmarking Hydrogen Evolving Reaction and Oxygen Evolving Reaction Electrocatalysts for Solar Water Splitting Devices. *J. Am. Chem. Soc.* **2015**, *137* (13), 4347–4357.
- (3) Nørskov, J. K.; Rossmeisl, J.; Logadottir, A.; Lindqvist, L.; Kitchin, J. R.; Bligaard, T.; Jónsson, H. Origin of the Overpotential for Oxygen Reduction at a Fuel-Cell Cathode. *J. Phys. Chem. B* **2004**, *108* (46), 17886–17892.
- (4) Hao, H.; Jin, B.; Liu, W.; Wu, X.; Yin, F.; Liu, S. Robust Pt@TiO<sub>x</sub>/TiO<sub>2</sub> Catalysts for Hydrocarbon Combustion: Effects of Pt-TiO<sub>x</sub> Interaction and Sulfates. *ACS Catal.* **2020**, *10* (22), 13543–13548.
- (5) Kamat, G. A.; Zamora Zeledón, J. A.; Gunasooriya, G. T. K. K.; Dull, S. M.; Perryman, J. T.; Nørskov, J. K.; Stevens, M. B.; Jaramillo, T. F. Acid Anion Electrolyte Effects on Platinum for Oxygen and Hydrogen Electrocatalysis. *Commun. Chem.* **2022**, *5* (1), 20.
- (6) Zhang, C.; Shen, X.; Pan, Y.; Peng, Z. A Review of Pt-Based Electrocatalysts for Oxygen Reduction Reaction. *Front. Energy* **2017**, *11* (3), 268–285.
- (7) Hansen, J. N.; Prats, H.; Toudahl, K. K.; Mørch Secher, N.; Chan, K.; Kibsgaard, J.; Chorkendorff, I. Is There Anything Better than Pt for HER? *ACS Energy Lett.* **2021**, *6* (4), 1175–1180.
- (8) Hughes, A. E.; Haque, N.; Northey, S. A.; Giddey, S. Platinum Group Metals: A Review of Resources, Production and Usage with a Focus on Catalysts. *Resources* **2021**, *10* (9), 93.
- (9) Yang, A.-C.; Choksi, T.; Streibel, V.; Aljama, H.; Wrasman, C. J.; Roling, L. T.; Goodman, E. D.; Thomas, D.; Bare, S. R.; Sánchez-Carrera, R. S.; Schäfer, A.; Li, Y.; Abild-Pedersen, F.;

- Cargnello, M. Revealing the Structure of a Catalytic Combustion Active-Site Ensemble Combining Uniform Nanocrystal Catalysts and Theory Insights. *Proc. Natl. Acad. Sci.* **2020**, *117* (26), 14721–14729.
- (10) Yang, A.-C.; Streibel, V.; Choksi, T. S.; Aljama, H.; Werghi, B.; Bare, S. R.; Sánchez-Carrera, R. S.; Schäfer, A.; Li, Y.; Abild-Pedersen, F.; Cargnello, M. Insights and Comparison of Structure–Property Relationships in Propane and Propene Catalytic Combustion on Pd- and Pt-Based Catalysts. *J. Catal.* **2021**, *401*, 89–101.
- (11) Dahl, S.; Logadottir, A.; Egeberg, R. C.; Larsen, J. H.; Chorkendorff, I.; Törnqvist, E.; Nørskov, J. K. Role of Steps in N<sub>2</sub> Activation on Ru(0001). *Phys. Rev. Lett.* **1999**, *83* (9), 1814–1817.
- (12) Greeley, J.; Mavrikakis, M. Alloy Catalysts Designed from First Principles. *Nat. Mater.* **2004**, *3* (11), 810–815.
- (13) Tripa, C. E.; Zubkov, T. S.; Yates, J. T.; Mavrikakis, M.; Nørskov, J. K. Molecular N<sub>2</sub> Chemisorption—Specific Adsorption on Step Defect Sites on Pt Surfaces. *J. Chem. Phys.* **1999**, *111* (18), 8651–8658.
- (14) Abild-Pedersen, F. Computational Catalyst Screening: Scaling, Bond-Order and Catalysis. *Catal. Today* **2016**, *272*, 6–13.
- (15) Ma, Z.; Cano, Z. P.; Yu, A.; Chen, Z.; Jiang, G.; Fu, X.; Yang, L.; Wu, T.; Bai, Z.; Lu, J. Enhancing Oxygen Reduction Activity of Pt-based Electrocatalysts: From Theoretical Mechanisms to Practical Methods. *Angew. Chem. Int. Ed.* **2020**, *59* (42), 18334–18348.
- (16) Marei, M. N.; Khan, H. A.; Badra, J. A.; Montoya, A.; Farooq, A.; Masri, A. R. Comparative Study of the Catalytic Oxidation of Hydrocarbons on Platinum and Palladium Wires and Nanoparticles. *Energy Fuels* **2022**, *36* (4), 2044–2057.

- (17) Shi, X.; Lin, X.; Luo, R.; Wu, S.; Li, L.; Zhao, Z.-J.; Gong, J. Dynamics of Heterogeneous Catalytic Processes at Operando Conditions. *JACS Au* **2021**, *1* (12), 2100–2120.
- (18) Toyao, T.; Maeno, Z.; Takakusagi, S.; Kamachi, T.; Takigawa, I.; Shimizu, K. Machine Learning for Catalysis Informatics: Recent Applications and Prospects. *ACS Catal.* **2020**, *10* (3), 2260–2297.
- (19) Ma, X.; Xin, H. Orbitalwise Coordination Number for Predicting Adsorption Properties of Metal Nanocatalysts. *Phys. Rev. Lett.* **2017**, *118* (3), 036101.
- (20) Calle-Vallejo, F.; Tymoczko, J.; Colic, V.; Vu, Q. H.; Pohl, M. D.; Morgenstern, K.; Loffreda, D.; Sautet, P.; Schuhmann, W.; Bandarenka, A. S. Finding Optimal Surface Sites on Heterogeneous Catalysts by Counting Nearest Neighbors. *Science* **2015**, *350* (6257), 185–189.
- (21) Abild-Pedersen, F.; Greeley, J.; Studt, F.; Rossmeisl, J.; Munter, T. R.; Moses, P. G.; Skúlason, E.; Bligaard, T.; Nørskov, J. K. Scaling Properties of Adsorption Energies for Hydrogen-Containing Molecules on Transition-Metal Surfaces. *Phys. Rev. Lett.* **2007**, *99* (1), 016105.
- (22) Mandal, S. C.; Abild-Pedersen, F. Classification of Adsorbed Hydrocarbons Based on Bonding Configurations of the Adsorbates and Surface Site Stabilities. *ACS Catal.* **2023**, *13* (20), 13663–13671.
- (23) Mamun, O.; Winther, K. T.; Boes, J. R.; Bligaard, T. A Bayesian Framework for Adsorption Energy Prediction on Bimetallic Alloy Catalysts. *Npj Comput. Mater.* **2020**, *6* (1), 177.
- (24) Roling, L. T.; Li, L.; Abild-Pedersen, F. Configurational Energies of Nanoparticles Based on Metal–Metal Coordination. *J. Phys. Chem. C* **2017**, *121* (41), 23002–23010.

- (25) Saini, S.; Halldin Stenlid, J.; Deo, S.; Plessow, P. N.; Abild-Pedersen, F. A First-Principles Approach to Modeling Surface Site Stabilities on Multimetallic Catalysts. *ACS Catal.* **2024**, *14* (2), 874–885.
- (26) Roling, L. T.; Abild-Pedersen, F. Structure-Sensitive Scaling Relations: Adsorption Energies from Surface Site Stability. *ChemCatChem* **2018**, *10* (7), 1643–1650.
- (27) Kulkarni, A.; Siahrostami, S.; Patel, A.; Nørskov, J. K. Understanding Catalytic Activity Trends in the Oxygen Reduction Reaction. *Chem. Rev.* **2018**, *118* (5), 2302–2312.
- (28) Kresse, G.; Hafner, J. *Ab Initio* Molecular Dynamics for Liquid Metals. *Phys. Rev. B* **1993**, *47* (1), 558–561.
- (29) Kresse, G.; Furthmüller, J. Efficiency of Ab-Initio Total Energy Calculations for Metals and Semiconductors Using a Plane-Wave Basis Set. *Comput. Mater. Sci.* **1996**, *6* (1), 15–50.
- (30) Kresse, G.; Furthmüller, J. Efficient Iterative Schemes for *Ab Initio* Total-Energy Calculations Using a Plane-Wave Basis Set. *Phys. Rev. B* **1996**, *54* (16), 11169–11186.
- (31) Hjorth Larsen, A.; Jørgen Mortensen, J.; Blomqvist, J.; Castelli, I. E.; Christensen, R.; Duřak, M.; Friis, J.; Groves, M. N.; Hammer, B.; Hargus, C.; Hermes, E. D.; Jennings, P. C.; Bjerre Jensen, P.; Kermode, J.; Kitchin, J. R.; Leonhard Kolsbjerg, E.; Kubal, J.; Kaasbjerg, K.; Lysgaard, S.; Bergmann Maronsson, J.; Maxson, T.; Olsen, T.; Pastewka, L.; Peterson, A.; Rostgaard, C.; Schiøtz, J.; Schütt, O.; Strange, M.; Thygesen, K. S.; Vegge, T.; Vilhelmsen, L.; Walter, M.; Zeng, Z.; Jacobsen, K. W. The Atomic Simulation Environment—a Python Library for Working with Atoms. *J. Phys. Condens. Matter* **2017**, *29* (27), 273002.
- (32) Wellendorff, J.; Lundgaard, K. T.; Møgelhøj, A.; Petzold, V.; Landis, D. D.; Nørskov, J. K.; Bligaard, T.; Jacobsen, K. W. Density Functionals for Surface Science: Exchange-Correlation Model Development with Bayesian Error Estimation. *Phys. Rev. B* **2012**, *85* (23), 235149.

- (33) Lee, K.; Murray, É. D.; Kong, L.; Lundqvist, B. I.; Langreth, D. C. Higher-Accuracy van Der Waals Density Functional. *Phys. Rev. B* **2010**, *82* (8), 081101.
- (34) Tahsini, N.; Yang, A.-C.; Streibel, V.; Werghi, B.; Goodman, E. D.; Aitbekova, A.; Bare, S. R.; Li, Y.; Abild-Pedersen, F.; Cargnello, M. Colloidal Platinum–Copper Nanocrystal Alloy Catalysts Surpass Platinum in Low-Temperature Propene Combustion. *J. Am. Chem. Soc.* **2022**, *144* (4), 1612–1621.
- (35) Monkhorst, H. J.; Pack, J. D. Special Points for Brillouin-Zone Integrations. *Phys. Rev. B* **1976**, *13* (12), 5188–5192.
- (36) Bengtsson, L. Dipole Correction for Surface Supercell Calculations. *Phys. Rev. B* **1999**, *59* (19), 12301–12304.
- (37) Winther, K. T.; Hoffmann, M. J.; Boes, J. R.; Mamun, O.; Bajdich, M.; Bligaard, T. Catalysis-Hub.Org, an Open Electronic Structure Database for Surface Reactions. *Sci. Data* **2019**, *6* (1), 75.
- (38) Yang, H.; Whitten, J. L. Dissociative Adsorption of H<sub>2</sub> on Ni(111). *J. Chem. Phys.* **1993**, *98* (6), 5039–5049.
- (39) Aireddy, D. R.; Ding, K. Heterolytic Dissociation of H<sub>2</sub> in Heterogeneous Catalysis. *ACS Catal.* **2022**, *12* (8), 4707–4723.
- (40) Fang, H.; Wu, S.; Ayvali, T.; Zheng, J.; Fellowes, J.; Ho, P.-L.; Leung, K. C.; Large, A.; Held, G.; Kato, R.; Suenaga, K.; Reyes, Y. I. A.; Thang, H. V.; Chen, H.-Y. T.; Tsang, S. C. E. Dispersed Surface Ru Ensembles on MgO(111) for Catalytic Ammonia Decomposition. *Nat. Commun.* **2023**, *14* (1), 647.
- (41) Cushing, G. W.; Navin, J. K.; Donald, S. B.; Valadez, L.; Johánek, V.; Harrison, I. C–H Bond Activation of Light Alkanes on Pt(111): Dissociative Sticking Coefficients,

- Evans–Polanyi Relation, and Gas–Surface Energy Transfer. *J. Phys. Chem. C* **2010**, *114* (40), 17222–17232.
- (42) Latimer, A. A.; Kulkarni, A. R.; Aljama, H.; Montoya, J. H.; Yoo, J. S.; Tsai, C.; Abild-Pedersen, F.; Studt, F.; Nørskov, J. K. Understanding Trends in C–H Bond Activation in Heterogeneous Catalysis. *Nat. Mater.* **2017**, *16* (2), 225–229.
- (43) Santoro, S.; Kozhushkov, S. I.; Ackermann, L.; Vaccaro, L. Heterogeneous Catalytic Approaches in C–H Activation Reactions. *Green Chem.* **2016**, *18* (12), 3471–3493.
- (44) Ferriday, T. B.; Middleton, P. H.; Kolhe, M. L. Review of the Hydrogen Evolution Reaction—A Basic Approach. *Energies* **2021**, *14* (24), 8535.
- (45) Yu, J.; Qin, X.; Yang, Y.; Lv, M.; Yin, P.; Wang, L.; Ren, Z.; Song, B.; Li, Q.; Zheng, L.; Hong, S.; Xing, X.; Ma, D.; Wei, M.; Duan, X. Highly Stable Pt/CeO<sub>2</sub> Catalyst with Embedding Structure toward Water–Gas Shift Reaction. *J. Am. Chem. Soc.* **2024**, *146* (1), 1071–1080.
- (46) Shao, M.; Chang, Q.; Dodelet, J.-P.; Chenitz, R. Recent Advances in Electrocatalysts for Oxygen Reduction Reaction. *Chem. Rev.* **2016**, *116* (6), 3594–3657.
- (47) Huang, L.; Zaman, S.; Tian, X.; Wang, Z.; Fang, W.; Xia, B. Y. Advanced Platinum-Based Oxygen Reduction Electrocatalysts for Fuel Cells. *Acc. Chem. Res.* **2021**, *54* (2), 311–322.
- (48) Daiane Ferreira Da Silva, C.; Claudel, F.; Martin, V.; Chattot, R.; Abbou, S.; Kumar, K.; Jiménez-Morales, I.; Cavaliere, S.; Jones, D.; Rozière, J.; Solà-Hernandez, L.; Beauger, C.; Faustini, M.; Peron, J.; Gilles, B.; Encinas, T.; Piccolo, L.; Barros De Lima, F. H.; Dubau, L.; Maillard, F. Oxygen Evolution Reaction Activity and Stability Benchmarks for Supported and Unsupported IrO<sub>x</sub> Electrocatalysts. *ACS Catal.* **2021**, *11* (7), 4107–4116.

- (49) Wu, H.; Wang, Y.; Shi, Z.; Wang, X.; Yang, J.; Xiao, M.; Ge, J.; Xing, W.; Liu, C. Recent Developments of Iridium-Based Catalysts for the Oxygen Evolution Reaction in Acidic Water Electrolysis. *J. Mater. Chem. A* **2022**, *10* (25), 13170–13189.
- (50) Mandal, S. C.; Das, A.; Roy, D.; Das, S.; Nair, A. S.; Pathak, B. Developments of the Heterogeneous and Homogeneous CO<sub>2</sub> Hydrogenation to Value-Added C<sub>2+</sub>-Based Hydrocarbons and Oxygenated Products. *Coord. Chem. Rev.* **2022**, *471*, 214737.
- (51) Peng, H.-J.; Tang, M. T.; Halldin Stenlid, J.; Liu, X.; Abild-Pedersen, F. Trends in Oxygenate/Hydrocarbon Selectivity for Electrochemical CO(2) Reduction to C<sub>2</sub> Products. *Nat. Commun.* **2022**, *13* (1), 1399.
- (52) Friedel, J. *The Physics of Metals*; Cambridge University Press: London, 1969.

## Table of Contents Entry

